JOURNAL OF SYNCHROTRON RADIATION
ISSN 1600-5775

X-ray diffraction reveals blunt-force loading threshold for nanoscopic structural change in *ex vivo* neuronal tissues

Joseph Orgel,[a]* Rama S. Madhurapantula,[a]* Ashley Eidsmore,[b] Meng Wang,[a] Pavel Dutov,[a] Charles D. Modrich,[a] Olga Antipova,[c] Jason McDonald[b] and Sikhanda Satapathy[b]

[a]Departments of Biology, Physics and Biomedical Engineering, Illinois Institute of Technology, Chicago, IL, USA, [b]Weapons and Materials Research Directorate, Army Research Laboratory, USA, and [c]X-ray Science Division, Argonne National Laboratory, Chicago, IL, USA. *Correspondence e-mail: orgel@iit.edu, rmadhura@iit.edu

Received 17 July 2018
Accepted 23 October 2018

Edited by V. Favre-Nicolin, CEA and Université Joseph Fourier, France

Keywords: blunt-force; *ex vivo*; myelin; loading; X-ray diffraction.

Supporting information: this article has supporting information at journals.iucr.org/s

An *ex vivo* blunt-force loading experiment is reported that may, in the future, provide insight into the molecular structural changes occurring in load-induced conditions such as traumatic brain injury (TBI). TBI appears to manifest in changes in multiple structures and elements within the brain and nervous system. Individuals with a TBI may suffer from cognitive and/or behavioral impairments which can adversely affect their quality of life. Information on the injury threshold of tissue loading for mammalian neurons is critical in the development of a quantified neuronal-level dose-response model. Such a model could aid in the discovery of enhanced methods for TBI detection, treatment and prevention. Currently, thresholds of mechanical load leading to direct force-coupled nanostructural changes in neurons are unknown. In this study, we make use of the fact that changes in the structure and periodicity of myelin may indicate neurological damage and can be detected with X-ray diffraction (XRD). XRD allows access to a nanoscopic resolution range not readily achieved by alternative methods, nor does the experimental methodology require chemical sample fixation. In this study, XRD was used to evaluate the affects of controlled mechanical loading on myelin packing structure in *ex vivo* optic nerve samples. By using a series of crush tests on isolated optic nerves a quantified baseline for mechanical load was found to induce changes in the packing structure of myelin. To the authors' knowledge, this is the first report of its kind.

1. Introduction

The determination of injury thresholds for neuronal tissues is critical to the development of a quantified mechanical dose-response model of the human brain that accounts for sub-neuronal damage. This type of damage is currently 'invisible' to commonly used visualization techniques. Current finite-element-based computational models compute temporal stress distributions once material properties and loading conditions are specified. However, lack of meaningful damage criteria for brain tissue at the nanoscopic level impedes the prediction of mild/moderate traumatic brain injury (TBI) outcome from computed stresses, *i.e.* the changes induced occur at a level that has not been detectable previously. Therefore a repeatable and quantitative measure of structural change that is meaningful in the context of TBI, observed under varied mechanical loading, is highly likely to be of future benefit to predicting the outcomes of injuries that lead to mild/moderate TBI.

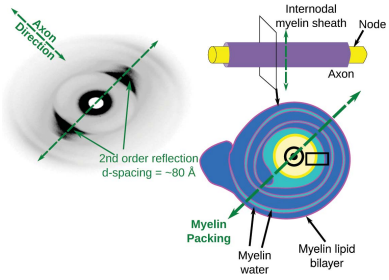

Recent experimental studies suggest that myelin pathology plays a key role in the severity of behavioral outcomes post-TBI, indicating the need for a quantified sub-neuronal load–structure change relationship. In a study on collegiate hockey players, myelin water fraction (intra and extracellular water in neurons in the brain) was transiently reduced in players diagnosed with concussion while there was no apparent reduction in players without concussion (Wright *et al.*, 2016). Another clinical study showed that individuals who had widespread myelin damage (myelin 'loosening') performed poorly on cognition tests and were more likely to sustain chronic concussive symptoms in response to injury (Dennis *et al.*, 2015). This indicates a correlation between sub-neuronal change and behavioral change. Furthermore, breakdown of the axon and myelin sheath has been observed to occur in both blunt and blast trauma victims, implying there may be a similar failure mechanism for different loading conditions between different modes of injury (McKee & Robinson, 2014). Animal studies on white matter damage and repair have provided insight into the process of demyelination and remyelination (Mierzwa *et al.*, 2015). Thus, load-induced alterations to the structure of animal myelin may be an indicator of concussive outcome in animal models. If this is the case, as the literature appears to indicate, then the data from quantified sub-neuronal load–structure change studies such as that reported here would make useful criteria for the diagnosis of TBI.

Observing the effects of mechanical loading on neuronal sub-cellular structures requires the sensitivity to detect nanometre-scale changes without imposing method-induced artifacts of a similar or larger size. Additionally, since dynamic loading produces transient stresses which travel away from the site of impact, it is important to observe changes throughout the impacted specimen. Such requirements make selection of an appropriate imaging method challenging. Methods such as two-photon microscopy and magnetic resonance imaging (MRI) allow large cross sections of tissue to be scanned but yield structural information at low spatial resolution (*e.g.* 11 T MRI machines $\sim$0.1 mm and two-photon imaging $\sim$1 µm scale resolution). In contrast, techniques such as electron microscopy and super-resolution optical microscopy can provide detailed spatial information close to or at the nanoscopic level but are impractical for scanning larger cross sections. Moreover, these techniques can introduce problematic changes, including shrinking, sample dehydration and protein cross-linking, as a result of standard sample preparation methods. The use of myelinated tissues, such as optic nerves, can be useful for understanding and establishing this dose-response model of loading. There have also been reports of perturbations to optic nerves in animal models of TBI (Wang *et al.*, 2011).

X-ray diffraction (XRD) has a long-demonstrated capability of detecting nanometre- to angström-level organization in samples with very limited sample preparation (Barrea *et al.*, 2014; Orgel & Irving, 2014; Yagi, 2011; Inouye *et al.*, 2014; Kirschner *et al.*, 1989; Liu *et al.*, 2016). This provides a means to study the complex problem of load-induced sub-cellular structural change in neuronal tissue without introducing sample preparation artifacts. To underscore this point, as we report here (see the *Results* and *Discussion* sections), data collected from chemically fixed (crosslinked) optic nerves indicate packing structure changes brought about by such fixation techniques. These results demonstrate the necessity of using non-fixed tissues in addition to techniques that not only do not introduce artifacts but are capable of studying the sensitive and nanometre-scale structural changes related to mild TBIs. XRD returns useful information regarding periodic structures at the nanoscopic scale and may also be utilized to scan larger cross sections. It is possible that mild TBI (the so-called 'invisible wound'), which is believed to be linked to smaller mechanical insults, involves correspondingly small changes to neuronal structures. The fact that these changes are not readily detectable by commonly used modalities gives explanation to the term 'invisible' wound. However, these small changes may be detected by XRD. This study provides support for these conjectures by presenting diffraction data showing quantifiable changes in myelin and possibly other sub-cellular structures from isolated optic nerves. These data also suggest a threshold for mechanical loading-induced sub-neuronal structural change.

2. Materials and methods

This study has assessed the structural integrity of neuronal myelin following mechanical loads applied *ex vivo*. Rat optic nerves were dissected and loaded using an impact device to examine how mechanical loading influences the periodicity and long-range ordering of myelin.

2.1. Optic nerve dissection

Non-diseased CD rats (Charles River Laboratories) between three and six months of age were generously donated by Dr. David McCormick (IIT Research Institute, Chicago, IL, USA). The rats were euthanized via pentobarbital induced coma prior to delivery in compliance with US Public Health Service Policy on Humane Care and Use of NA Care and Use of Laboratory Animals. Optic nerves were carefully dissected, immediately following euthanasia, after exposing the brain by cutting the cranium open. The samples were impacted (loaded) immediately (<20 min) following dissection. After samples were impacted they were immediately mounted and sealed between sheets of thin mica (thickness <50 µm). XRD data were acquired following impact and mounting. No significant differences were detected in myelin spacing over a time span of 12 h, after loading the samples into the mica sandwich [see Fig. S5 of the supporting information (SI)]. All samples reported here were mounted onto sample chambers within 2 h of impact loading.

2.2. Chemical fixation of optic nerves

In addition to non-fixed optic nerve controls (unimpacted) for the nerve injury model (Section 2.3), unimpacted (no load applied) optic nerves were fixed by immersion in 2.5% (*w*/*v*)

glutarldehyde in phosphate buffered saline (PBS) for 5 min. These samples were then transferred and sealed between two thin (<50 µm thick) mica sheets, with some PBS around the tissue. The sheets were sealed with epoxy glue on the sides to prevent dehydration during XRD data acquisition.

2.3. Optic nerve injury model

A custom-designed impact delivery system for delivering mechanical loads to optic nerve samples was constructed [Fig. 1(*a*)]. Impact was applied using a 'crush' force where the cylindrical impactor head (3 mm face diameter) was positioned to deliver a constant applied force perpendicular to the optic nerve (0.6 mm diameter) with a standard dwell time of 1 s using a stepper motor. All loading set points and measurements reported here are in grams (g). Optic nerves were laid out on a glass slide, which was placed on top of the sample mount (3D positioner stand). After impact, the samples were loaded onto mica mounts as described in the previous section. The tip of the impact head is designed to cover the entire area of the sample, to ascertain uniform impact. This is the only part of the apparatus that comes into direct contact with the sample.

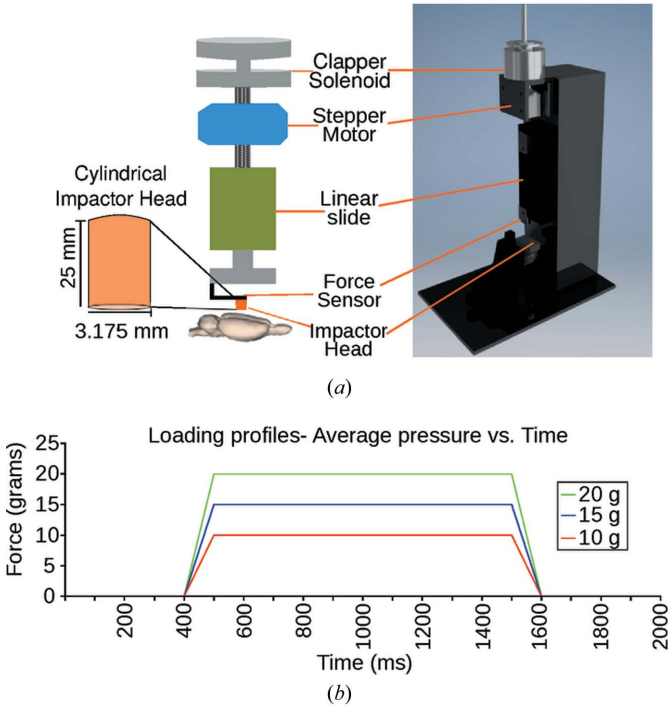

Figure 1
(*a*) Images of the blunt-impact loading apparatus. The stepper motor and clapper solenoid are attached by a threaded rod to a linear slide. The stepper is used for impact using a slow impact (as reported in this study) and the clapper solenoid was incorporated to be able to deliver 'accelerative' loading. A force sensor with the impact head is attached to the other end of the linear slide. The base for a glass slide, on which the optic nerve is placed for impact, is mounted on a 3D positioning stage. The motor or solenoid moves the linear slide downwards to impact the sample and dwell (when activated). The sample is represented as a rodent brain rather than optic nerve for purely illustrative purposes. All samples in this study were optic nerves. (*b*) Averaged applied loading curves. Impact loading was applied at the pressure (or force) set points demonstrated in the figure. The impactor dwell time was 1 s.

2.4. X-ray diffraction

X-ray diffraction experiments were carried out at the Biophysics Collaborative Access Team (BioCAT) at the Advanced Photon Sources, Argonne National Laboratory, Chicago, IL, USA (see SI Section S1 and SI Fig. S1 for further details on the beamline setup).

3. Results

3.1. Annotation of XRD patterns

Previous works describing XRD patterns from myelinated nerves fibers and single nerves were referenced for our study (Kirschner *et al.*, 1989; Inouye *et al.*, 2014). In our study data, X-ray reflections from myelin were identified (by spacing and orientation, relative to the sample) in diffraction patterns from optic nerves.

The myelin sheath is essentially a spiral infolding around an axon. Its structure consists of a periodic arrangement of membrane pairs with embedded proteins separated by aqueous spaces about 5 nm thick (Siegel, 2006). The repeat period for the membrane packing in native myelin is typically found to lie between 150 and 185 Å (Fernandez-Moran & Finean, 1957; Kirschner *et al.*, 1989), commonly 160 Å in the central nervous system. A native spacing between the myelin layers is maintained through the balance of various forces including the following: van der Waals attraction due to fluctuating charges, electrostatic repulsion from fixed ions, and repulsion due to inter-membrane water. The embedded proteins also play a role in maintaining the larger spacing seen in myelin in comparison with that observed in pure lipids (Cotter *et al.*, 2010). The ordering of phospholipid bilayers within these myelin laminae gives rise to an alternating 'step-function' of electron densities which leads to a strong diffraction series (Fig. 2). In particular, second- and fourth-order reflections are seen with *d*-spacings of 80 Å and 40 Å and are believed to originate from the mean distance from the center of one myelin layer to the next (Siegel, 2006).

3.2. Effects of tissue fixation on recorded *d*-spacing

It is currently common practice to embed and fix tissue samples prior to post-mortem evaluation in TBI studies. In preliminary experiments using glutaraldehyde fixation we found that the sample preparation methods introduced changes to the lamellar packing of myelin that were as great as or greater than those following applied mechanical load (between 5 and 25%). These observations led to the conclusion that the glutaraldehyde fixation method should be abandoned in future studies where the objective is to measure small-scale change; Fig. 3 shows a comparison of representative diffraction patterns between non-fixed and glutaraldehyde-fixed optic nerve. A ∼20% (∼15 Å) change is seen in the second-order *d*-spacing in glutaraldehyde-fixed samples in comparison with fresh (unfixed) samples. Mean and stan-

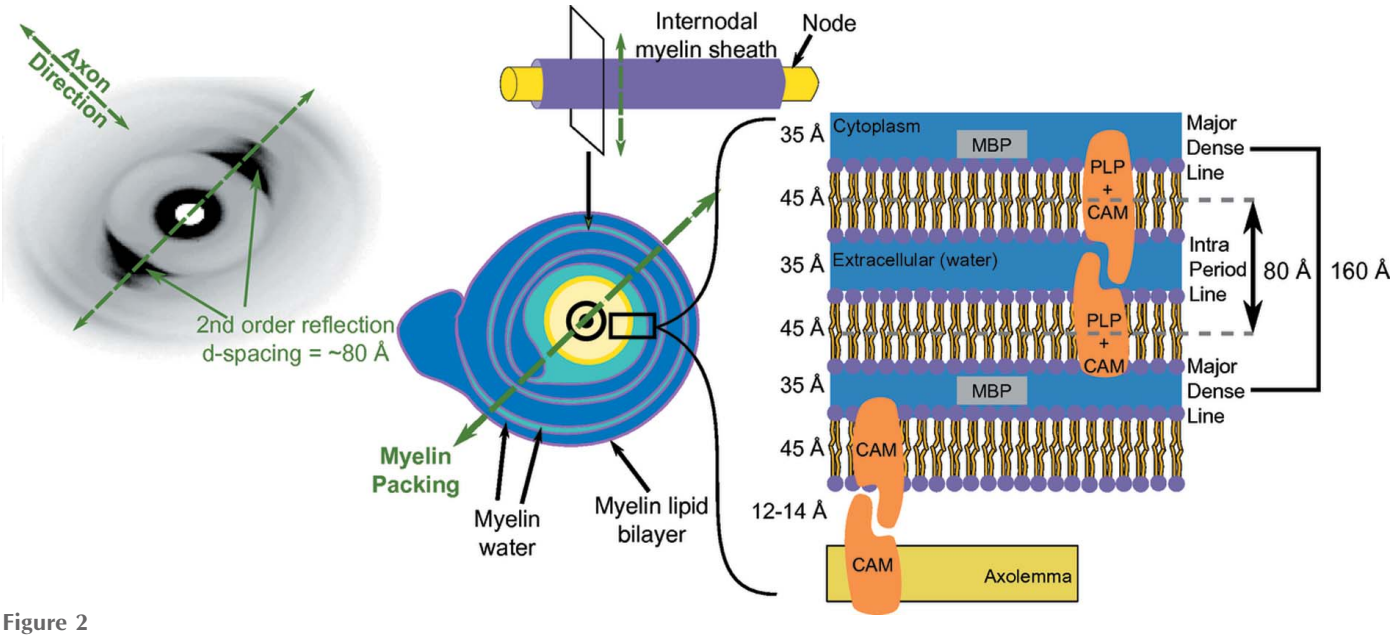

Figure 2
X-ray diffraction pattern from myelin. This annotated X-ray diffraction pattern from a myelinated mammalian nerve provides a visual reference. The (radial) myelin elements are identified from diffraction appearing on a 160 Å primary spacing repeating at 79.39 Å for its second order. It is orientated at 90° to the neuron axonal long axis. A distinct diffraction element at ∼90° to the labeled myelin diffraction is observed at 78.24 Å and either originates from fibrous structures along the neurons axonal axis or from obliquely orientated nodal myelin [that is, obliquely oriented relative to the radial myelin as shown by Inouye *et al.* (2014)]. In either case, the diffraction spacing is distinctly different from that of the main, strongest, diffraction of the neuron (the myelin diffraction labeled in this figure). Neuron structural representations were adapted from Fletcher & Mullins (2010) and Siegel (2006).

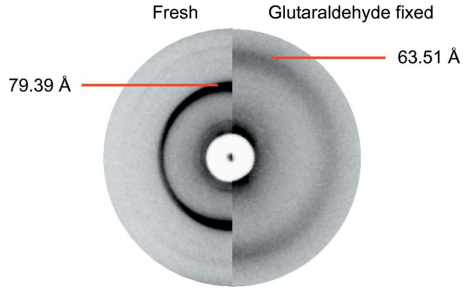

Figure 3
Representative comparison of XRD patterns from untreated (left) and glutaraldehyde fixed (right). The second order of myelin and respective *d*-spacing is marked with arrows. Note the decreased diffraction signal and coherence in the fixed sample relative to the freshly dissected, untreated sample.

dard deviations on multiple data points from glutaraldehyde-fixed samples are presented in SI Table S1.

3.3. Impact loading

The loading curves used are shown in Fig. 1(*b*). These loading profiles, with an impactor dwell time of 1 s, resulted in force loads of 10, 15 and 20 g resulting in nominal average pressures of 1.8, 2.7 and 3.6 psi across the impactor face in contact with the optic nerve. For each of the four loading conditions (control, 10, 15, 20 g), five optic nerves, each extracted from a separate specimen, were analyzed (see SI Table S1 for details). For each sample, diffraction patterns were recorded at 20 observation points within the region of impact. Representative diffraction patterns are shown in Fig. 4. The mean and standard deviations of myelin second- and fourth-order *d*-spacings were calculated for each loading condition group. Calculations are visualized in Fig. 5, with the precise values given in SI Tables S1 and S2.

3.4. Optic nerve injury model

Optic nerve samples were impact-loaded immediately following post-mortem extraction. The nerve was mechanically loaded and XRD data were recorded at 20 different locations, in a snake-like pattern, in the impacted region (the region of tissue directly under the impactor head). Data from five samples were recorded for the control and each loading condition. Statistics on these samples are presented in SI Table S1.

From the data presented here, we observe in native myelin (control sample) a strong second-order reflection which corresponds to a *d*-spacing of about 79–80 Å. This value is consistent with the 80 Å value reported in the literature (Siegel, 2006). This strong *d*-spacing is maintained at 79–80 Å for each of the groups receiving an average impact force up to and including 15 g. In contrast, at an average delivered force of 20 g, the expressed average myelin *d*-spacing significantly reduces to 76.74 Å. Furthermore, a loss of intensities for strong myelin reflections was observed above a force of 15 g, as seen in Fig. 4, which may correspond to a loss of long-range order. The fourth-order myelin peak is observed to split beyond the control and 10 g loading, partly accounting for the wider range of recorded *d*-spacing in both the second and fourth orders (not seen in the second order due to its broader and lower resolution character). Both split peaks of the fourth order show a related response to loading (Figs. S2 and S3) and,

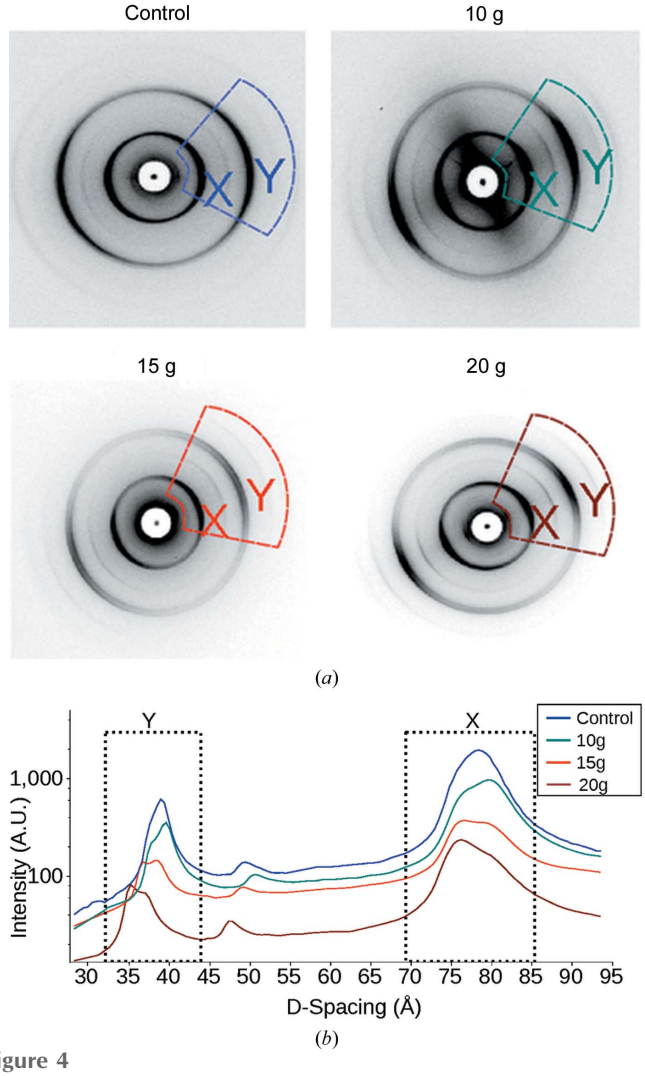

Figure 4
(*a*) Diffraction patterns and (*b*) integrated data (intensity *versus* *d*-spacings) of control and impact-loaded rat optic nerve samples. The intensity profiles were extracted by radially integrating all data. Highlighted sectors indicated in (*a*) are used to draw attention to the reflections under discussion. The dashed rectangles in (*b*) indicate peaks *X* and *Y*, respectively. See SI Fig. S2 for Gaussian peak fitting and the positions where these the peaks were detected and used for further analyses.

although it is possible that there is a two-step myelin response to loading (such as inner and outer myelin layer response to load) to avoid over-interpretation of our data, we have taken the average of the split peaks (via the peak fitting algorithm, see Fig. S2) for statistical analysis (Fig. 5, SI Fig. S5 and SI Tables S1 and S2). Even with this approach, there appears to be a marginally significant change at 15 g and a very significant change at 20 g. We have chosen to remain conservative and observe that a noticeable change to myelin structure occurs between delivered impactor forces of 15 and 20 g.

4. Discussion

Recent studies highlight the role myelin plays in cognition and suggest a better understanding of the evolution of nanostructural changes in myelin following mechanical insult. These insights may aid in the prediction of resulting injury scenarios such as TBI and chronic traumatic encephalopathy (Wright *et al.*, 2016; Dennis *et al.*, 2015; Armstrong *et al.*, 2015). Changes in myelin orientation and Wallerian degeneration in response to impact have been described in previous works (Armstrong *et al.*, 2016). However, the extent of damage at a nanoscopic level (*i.e.* changes to the molecular organization of myelin) immediately following mechanical loading is not well understood. The identification of and the manner by which small, mechanically disturbed structures foster chronic neurodegenerative effects is also not clear, largely due to the challenge in observing these structures at high enough resolution in tissue samples not significantly altered from their native state (by sample preparations that may be required for observational techniques or otherwise).

Through use of X-ray fiber diffraction, this study demonstrates evident changes to myelin structure that occur following applied mechanical load in post-mortem isolated optic nerves. These changes are reproducible and are evident following low levels of loading. Specifically, in optic nerve samples loaded over a 1 s duration, a noticeable change to the myelin packing structure first occurred at an average applied force between 15 and 20 g (2.7 to 3.6 psi average pressure across the impactor head). It is possible that there is a first

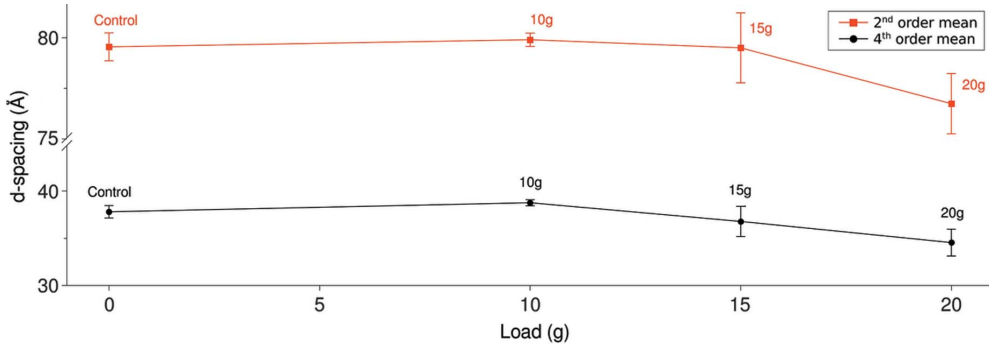

Figure 5
Average second- and fourth-order *d*-spacing for myelin from impact-loaded specimens and controls. Each load is represented and plotted in relation to its corresponding average applied impactor force (0 g control, 10, 15, 20 g). Standard deviation bars are representative of the difference between observations in each loading or control group. The general trend observed is a reduction in *d*-spacing of myelin with increasing load. The increasing standard deviation demonstrates another measure of disturbance to molecular structure as a result of increasing load.

structural change at 15 g (Fig. 5 and SI Fig. S4) (such as outer myelin disruption, distal to the cytoskeleton) and a more significant change at 20 g where the cytoskeleton supported/proximal side of the myelin is disrupted or further disrupted to the degree that it is more significantly detected; see SI *Results and Discussion* section. Taking these observations together, we believe that the observed decrease in the spacing of myelin layers (as revealed by the reduced *d*-spacing of its diffraction) is most readily explained as the result of reduced water content between the membrane layers. Possible scenarios leading to this include the outflow of water from between the layers of myelin or compromise to embedded structural proteins leading to slight collapse of myelin packing and subsequent water outflow. We hypothesize that these forms of disturbance would potentially have further impact on extracellular protein structures necessary for myelin maintenance (Gupta *et al.*, 2005) such as axo-glial cellular adhesion molecules, including neurexin, neuroligin and nectin-like molecules located in the narrow gap between the axonal membrane and the surrounding myelin sheath (Przekwas *et al.*, 2016). Such disturbances would further compromise long-term capability for restructure and thus foster an increased risk for chronic injury outcome. We acknowledge that further study is needed to identify the timing of such events and their corresponding force dependencies.

Furthermore, while differences exist between rat and human optic nerves, the overall molecular packing structure of the myelin sheath is somewhat similar. This serves for the purposes of this study: the detection of a threshold applied force to change the myelin structure. In terms of these experimental data, differences between species are irrelevant as only a single species was made use of here. Some characteristic differences include diameter (201 ± 1 µm in rats versus 1580 ± 210 µm in humans) and the faint presence of the lamina cribrosa in the rat, while it is fully developed in humans (Chen *et al.*, 2016). However, our XRD data from rat optic nerves show a base periodicity of ∼159 Å, which is almost identical to that reported from human cerebral tissue (166.7 ± 0.09 Å in males and 165.0 ± 0.03 Å in females) (De Felici *et al.*, 2008). Similar evidence has also been noted for mouse and rabbit optic nerve samples by Denninger *et al.* (2014). Collection of data from human tissues will be a necessary next step to experimentally determine, rather than infer from similarities in structure, the structure (and presumably injury) to applied force relationship in humans and therefore in traumatically induced injuries.

The current study validates the use of X-ray diffraction as a viable approach to study myelin damage as a result of traumatically induced injury, such as that found in TBI. The nanoscopic resolution range that is important for studying these changes is readily accessible with the use of X-rays. With the advent of synchrotron X-ray scanning modalities, it is now possible to scan large sections of brain tissues to record myelin diffraction and calculate the changes in *d*-spacing across these sections post-TBI. These data can be interpreted in the purview of microscopic observations of myelin reformation and rearrangement and resulting functional loss reported previously (Jones *et al.*, 2012; Ramaswamy *et al.*, 2005; Kozlowski, 2011). Based on these observations, we hypothesize that myelin damage over time as observed in animals and patients suffering from TBI may be a result of the initial damage caused by the impact itself and the accrued effects of this 'nucleation'. A further study into the local and long-range changes in myelin structure in the brains of animals inflicted with TBI (controlled cortical impact) may lead to further insights into the process of myelin degeneration as a result of mechanical insult. This information is vital to developing protective gear to prevent such damage and therapeutic regimens to treat the effects of such injuries. This study lays some of the groundwork by sensitively detecting at what mechanical loads impact-induced nano-structural changes occur to myelin in isolated neurons.

5. Related literature

The following references, not cited in the main body of the paper, have been cited in the supporting information: Benecke *et al.* (2014); Hammersley (1997).

Acknowledgements

The authors thank the staff and scientists of the BioCAT group.

Funding information

This project was supported by grant 9 P41 GM103622 from the National Institute of General Medical Sciences of the National Institutes of Health. This material is based upon work supported by, or in part by, the US Army Research Laboratory and the US Army Research Office under contract/grant number W911NF-11-2-0018-P00002 to JO). This research used resources of the Advanced Photon Source, a US Department of Energy (DOE) Office of Science User Facility operated for the DOE Office of Science by Argonne National Laboratory under Contract No. DE-AC02-06CH11357.

References

Armstrong, R. C., Mierzwa, A. J., Marion, C. M. & Sullivan, G. M. (2016). *Exp. Neurol.* **275**, 328–333.

Armstrong, R. C., Mierzwa, A. J., Sullivan, G. M. & Sanchez, M. A. (2015). *Neuropharmacology*, **110**, 654–659.

Barrea, R. A., Antipova, O., Gore, D., Heurich, R., Vukonich, M., Kujala, N. G., Irving, T. C. & Orgel, J. P. R. O. (2014). *J. Synchrotron Rad.* **21**, 1200–1205.

Benecke, G., Wagermaier, W., Li, C., Schwartzkopf, M., Flucke, G., Hoerth, R., Zizak, I., Burghammer, M., Metwalli, E., Müller-Buschbaum, P., Trebbin, M., Förster, S., Paris, O., Roth, S. V. & Fratzl, P. (2014). *J. Appl. Cryst.* **47**, 1797–1803.

Chen, L., Zhao, Y. & Zhang, H. (2016). *Vision*, **1**, 4.

Cotter, L., Özçelik, M., Jacob, C., Pereira, J. A., Locher, V., Baumann, R., Relvas, J. B., Suter, U. & Tricaud, N. (2010). *Science*, **328**, 1415–1418.

De Felici, M., Felici, R., Ferrero, C., Tartari, A., Gambaccini, M. & Finet, S. (2008). *Phys. Med. Biol.* **53**, 5675.

Denninger, A. R., Demé, B., Cristiglio, V., LeDuc, G., Feller, W. B. & Kirschner, D. A. (2014). *Acta Cryst.* D**70**, 3198–3211.

Dennis, E. L., Ellis, M. U., Marion, S. D., Jin, Y., Moran, L., Olsen, A., Kernan, C., Babikian, T., Mink, R., Babbitt, C., Johnson, J., Giza, C. C., Thompson, P. M. & Asarnow, R. F. (2015). *J. Neurosci.* **35**, 10202–10211.
Fernandez-Moran, H. & Finean, J. B. (1957). *J. Cell Biol.* **3**, 725–748.
Fletcher, D. A. & Mullins, R. D. (2010). *Nature*, **463**, 485.
Gupta, R., Truong, L., Bear, D., Chafik, D., Modafferi, E. & Hung, C. T. (2005). *J. Orthop. Res.* **23**, 1232–1239.
Hammersley, A. P. (1997). *FIT2D: An Introduction and Overview*. ESRF Internal Report ESRF97HA02T. European Synchrotron Radiation Facility, Grenoble, France.
Inouye, H., Liu, J., Makowski, L., Palmisano, M., Burghammer, M., Riekel, C. & Kirschner, D. A. (2014). *PLoS One*, **9**, e100592.
Jones, T. A., Liput, D. J., Maresh, E. L., Donlan, N., Parikh, T. J., Marlowe, D. & Kozlowski, D. A. (2012). *J. Neurotrauma*, **29**, 1455–1468.
Kirschner, D. A., Inouye, H., Ganser, A. L. & Mann, V. (1989). *J. Neurochem.* **53**, 1599–1609.
Kozlowski, D. (2011). *Neural Plasticity and Neurorehabilitation Following Traumatic Brain Injury*. Technical Report W81XWH-08-1-0624. DTIC Document. DePaul University Chicago, IL 60604, USA.
Liu, J., Costantino, I., Venugopalan, N., Fischetti, R. F., Hyman, B. T., Frosch, M. P., Gomez-Isla, T. & Makowski, L. (2016). *Sci. Rep.* **6**, 33079.
McKee, A. C. & Robinson, M. E. (2014). *Alzheimer's Dementia*, **10**, S242–S253.
Mierzwa, A. J., Marion, C. M., Sullivan, G. M., McDaniel, D. P. & Armstrong, R. C. (2015). *J. Neuropathol. Exp. Neurol.* **74**, 218–232.
Orgel, J. P. R. O. & Irving, T. C. (2014). *Advances in Fiber Diffraction of Macromolecular Assembles*, in *Encyclopedia of Analytical Chemistry*, edited by R. A. Meyers, pp. 1–26 (doi:10.1002/9780470027318.a9420).
Przekwas, A., Somayaji, M. R. & Gupta, R. K. (2016). *Front. Neurol.* **7**, doi:10.3389/fneur.2016.00002.
Ramaswamy, S., Goings, G. E., Soderstrom, K. E., Szele, F. G. & Kozlowski, D. A. (2005). *Brain Res.* **1053**, 38–53.
Siegel, G. J. (2006). Editor. *Basic Neurochemistry: Molecular, Cellular, and Medical Aspects*, 7th ed. Amsterdam: Elsevier.
Wang, J., Hamm, R. J. & Povlishock, J. T. (2011). *J. Neurotrauma*, **28**, 1185–1198.
Wright, A. D., Jarrett, M., Vavasour, I., Shahinfard, E., Kolind, S., van Donkelaar, P., Taunton, J., Li, D. & Rauscher, A. (2016). *PLoS One*, **11**, e0150215.
Yagi, N. (2011). *J. Phys. Conf. Ser.* **272**, 012009.